Neutron capture resonances in ^{142}Nd and ^{144}Nd

K. Wisshak,* F. Voss, and F. Käppeler
Forschungszentrum Karlsruhe, Institut für Kernphysik, Postfach 3640 D-76021 Karlsruhe, Germany
(Received 10 October 1997)

The neutron capture cross sections of ^{142}Nd and ^{144}Nd which were determined recently with the Karlsruhe 4πBaF$_2$ detector have been reanalyzed at low energies. The parameters of 52 resonances in ^{142}Nd and of 78 resonances in ^{144}Nd were extracted by means of a shape analysis program, yielding a more reliable determination of the averaged cross sections below 20 keV. This study confirms the previously reported stellar cross sections, so that the *s*-process study based on these data remains unchanged. [S0556-2813(98)03706-6]

PACS number(s): 25.40.Lw, 26.20.+f, 27.60.+j, 98.80.Ft

I. INTRODUCTION

The experimental situation of neutron capture in neodymium isotopes is quite peculiar. With six reported measurements per isotope, neodymium is one of the most frequently investigated elements. However, for each isotope the individual results differ by factors of 2–3 [1]. Hence, a reliable set of cross sections is urgently required for *s*- and *r*-process studies [2].

In an attempt to improve the experimental data, the neutron capture cross sections of the six neodymium isotopes ^{142}Nd, ^{143}Nd, ^{144}Nd, ^{145}Nd, ^{146}Nd, and ^{148}Nd were measured using the Karlsruhe 4πBaF$_2$ detector for registration of capture events [2]. Compared to previous results, a five times better accuracy could be achieved for the stellar cross sections at $kT=30$ keV, and, for the first time, reliable values were also obtained at lower temperatures for a complete set of isotopes. With these data the *s*-process abundances of the neodymium isotopes could be described quantitatively.

In this study, the differential capture cross sections of ^{142}Nd and ^{144}Nd were measured with sufficient resolution that single resonances could be resolved up to about 20 keV neutron energy. Despite this feature, the stellar cross sections were first determined by averaging the observed capture yield [2]. This simplification may be justified to good approximation according to a similar study on ^{134}Ba [3] and on three tin isotopes [4]. On the other hand, the cross section at these low energies could be affected by the treatment of a significant background due to the capture of scattered neutrons. The isotopes ^{144}Nd and ^{145}Nd are particularly sensitive in this respect due to their extremely large *s*-wave strength function, that is exceeded only by a few isotopes in the mass range around $A=50$ [5]. Therefore, the response of the experimental setup to scattered neutrons is rather critical for a reliable determination of the comparably small (n,γ) cross section of ^{144}Nd.

The present work deals with a reanalysis of the cross sections reported in Ref. [2] by means of a shape analysis program for determining the resonance parameters. From these parameters new and more reliable data for the low energy part of the stellar cross sections were derived, an improvement, that is especially important, since stellar model calculations indicate that most of the *s* process proceeds via the ^{13}C$(\alpha,n)^{16}$O reaction at thermal energies of 10 keV or less [6,7].

II. EXPERIMENT AND DATA EVALUATION

Experiment and data analysis have been described in detail in Ref. [2]. Continuous neutron spectra were produced via the ^{7}Li$(p,n)^7$Be reaction using the pulsed proton beam of the Karlsruhe 3.75 MV Van de Graaff accelerator. Capture events were registered with the Karlsruhe 4πBaF$_2$ detector [8] with a time resolution of about 1 ns. The samples, enriched to 95.5% in ^{142}Nd and 82.1% in ^{144}Nd, were located at a neutron flight path of 78 cm. The sample mass was 7.0 and 7.4 g, and the thickness 6.3 and 5.5×10^{-3} A/b, respectively. Four runs were performed with different maximum neutron energies and acquisition modes [2]. All time-of-flight (TOF) spectra could be analyzed down to a minimum neutron energy of 3 keV, but the run with 200 keV maximum neutron energy was omitted in the present analysis due to its smaller signal to background ratio at low energies.

After summation of the capture yields from the three other runs, the resulting TOF spectra were analyzed with the FANAC code [9] in the same way as described for ^{134}Ba [3]. The global input parameters like strength functions or nuclear radii were the same as in the calculations of the multiple scattering and self-shielding corrections described in Ref. [2]. Known neutron widths of *s*- and *p*-wave resonances as well as resonance spins were adopted from the JENDL-3 evaluation [10].

The TOF measurement of the neutron energy is determined by the pulse width of the proton beam (0.7 ns), the time resolution of the 4πBaF$_2$ detector (0.5 ns), and the sample thickness (4.6 mm), resulting in an average resolution in neutron energy of ±55 eV at 10 keV, ±35 eV at 7 keV, and ±23 eV at 5 keV. Thus, the shape of the very broad *s*-wave resonances is to a large extent determined by the experimental resolution which means that it was not possible to derive the individual resonance parameters Γ_n or Γ_γ directly from the present experiment. Instead, the resonance area $A_\gamma=g\Gamma_n\Gamma_\gamma/(\Gamma_n+\Gamma_\gamma)$ was determined in the fits.

If no information on Γ_n is available, the average neutron width can be calculated via the relation [11]

*Author to whom correspondence should be addressed.

TABLE I. Areas of capture resonances in ^{142}Nd.

Resonance energy (keV)		g	l	$g\Gamma_n$ [a]	Resonance area [b] (meV)		
Ref. [10]	This work			(meV)	This work	Ref. [5]	Ref. [10]
3.271	3.277	1	1	64	24.6 ± 2.7	15	25.1
3.382	3.391		0	343	56.0 ± 4.8	38	38.2
3.996	3.993		0	828	51.9 ± 5.2	47	45.6
4.145	4.142	1	1	85	20.0 ± 3.1	22	28.5
4.510		1	1	27		1.8	13.0
4.532	4.540		0	7572	49.5 ± 6.6	44	42.5
5.063	5.054	2	1	78	39.4 ± 2.6	40	41.1
5.156	5.152	2	1	90	38.7 ± 2.4	47	44.3
5.426	5.414	2	1	98	50.8 ± 2.7	50	45.9
5.491	5.475 [c]		0	3305	50.7 ± 5.1	41	39.6
5.958	5.951 [c]	1	1	38	7.9 [e]	3.7	17.9
5.982	5.965		0	1437	45.5 ± 4.6	44	42.6
6.236	6.225	2	1	122	51.0 ± 3.0	58	50.9
6.927	6.905		0	575	69.5 ± 7.5	47	45.8
6.955	6.935 [c]	1	1	72	23.3 ± 4.8	18	26.6
7.246	7.217		0	548	50.6 ± 4.2	45	43.8
	7.627		0	600 [d]	82.1 ± 4.9		
8.261	8.231		0	533	39.4 ± 2.2	32	31.0
8.423	8.392		0	1944	51.5 ± 2.6	45	43.5
8.806	8.767	2	1	284	71.2 ± 2.0	64	56.6
9.019	8.974		0	192	123.8 ± 2.7	47	53.3
9.840	9.793 [c]	2	1	290	59.1 ± 5.6	70	61.6
9.885	9.841 [c]		0	11840	84.1 ± 8.9	64	61.9
10.15	10.11	2	1	540	84.2 ± 3.9	78	70.9
10.30	10.24 [c]	1	1	66	30.6 ± 3.3	16	25.1
10.96	10.91		0	10540	51.6 ± 5.0	43	41.6
11.14	11.09 [c]	2	1	90	51.4 ± 3.4	46	43.8
11.26	11.20 [c]	1	1	109	31.9 ± 3.4	27	31.1
11.49	11.42	1	1	210	39.6 ± 3.6	36	36.4
12.94	12.86	2	1	526	86.4 ± 6.3	84	75.9
13.45	13.37 [c]	2	1	96	59.9 ± 5.7	49	45.4
13.52	13.46 [c]		0	4282	98.4 ± 16.5	84	81.3
13.66	13.58 [c]		0	89450	134 ± 16	234	226.2
14.27	14.18	1	1	190	46.4 ± 6.3	35	35.8
14.49	14.40	2	1	112	60.5 ± 5.6	55	48.9
14.99	14.93 [c]	1	1	52	10.4 [e]	10	22.5
15.07	14.98	2	1	174	68.6 ± 6.4	68	58.4
15.46	15.36 [c]		0	12890	43.2 ± 4.4	43	41.6
15.66	15.56	2	1	106	67.1 ± 3.2	53	47.7
15.94	15.83	2	1	254	68.6 ± 3.6	87	75.0
16.26	16.15 [c]		0	54290	56.1 ± 7.6	91	88.0
16.36	16.25 [c]	2	1	346	70.1 ± 5.6	82	72.3
17.07	16.96	2	1	1360	76.2 ± 3.8	89	83.5
17.36	17.24	2	1	114	61.8 ± 3.5	56	49.6
18.09	17.95	1	1	351	45.3 ± 4.8	40	39.3
19.09	18.95 [c]	2	1	280	76.3 ± 5.5	77	67.2
19.27	19.13 [c]	1	1	103	16.7 ± 9.2	26	30.5
19.37	19.23 [c]		0	46580	77.2 ± 13.8	78	77.7
19.63	19.48 [c]	1	1	78	5.7 ± 4.2	20	27.8
19.96	19.81 [c]	2	1	106	52.8 ± 4.1	53	47.7
20.23	20.08 [c]	2	1	212	89.9 ± 4.7	100	87.4
20.48	20.41 [c]	2	1	144	81.2 ± 4.4	50	46.0
20.66						70	60.2
20.83	20.71 [c]	1	1	85	25.7 ± 4.1	21	27.9
20.90						23	29.0

[a]Values for g, l, and $g\Gamma_n$ adopted from the JENDL-3 evaluation.

[b]$A_\gamma = g\Gamma_n\Gamma_\gamma/(\Gamma_n+\Gamma_\gamma)$.

[c]Resonance energy was taken as fixed parameter.

[d]Adopted value.

[e]Adopted as fixed parameter from Ref. [12].

TABLE II. Areas of capture resonances in ^{144}Nd.

Resonance energy (keV)		g	l	$g\Gamma_n$ [a]	Resonance area [b] (meV)		
Ref. [10]	This work			(meV)	This work	Ref. [5]	Ref. [10] [c]
2.762	2.776		0	4091	111.0 ± 7.9	63	61.0
2.955	2.958	1	1	60	24.9 ± 2.1	13.5	24.4
3.063		1	1	44		3.0	21.2
3.293		1	1	45		4.2	21.5
3.538	3.553		0	15940	45.6 ± 9.1	43	41.6
3.631		1	1	42		1.0	20.7
	3.677	1	1	84 [d]	24.4 ± 3.2		
3.749	3.752 [e]		0	1386	47.1 ± 10.3	26	25.1
3.762	3.766	1	1	55	28.2 ± 5.6	11	23.5
4.239	4.240	1	1	54	28.8 ± 3.2	10	23.2
4.598	4.611	1	1	130	42.9 ± 3.6	29	31.1
4.738	4.748		0	305	79.1 ± 9.5	28	27.3
4.929	4.937 [e]		0	24370	83.2 ± 12.6	67	64.8
4.954	4.962 [e]	1	1	207	49.4 ± 8.1	34	34.2
5.147	5.148	1	1	74	35.6 ± 3.3	19	26.4
5.648	5.660		0	3398	68.0 ± 10.9	39	37.7
5.843	5.862	1	1	85	67.7 ± 6.2	22	27.7
6.106	6.106 [e]		0	13530	85.9 ± 18.6	62	59.9
6.138	6.127 [e]	1	1	100	36.2 ± 10.5	25	29.0
6.747	6.730 [e]	1	1	74	25.7 ± 7.6	19	26.4
6.778	6.778 [e]	2	1	116	47.3 [f]	55	48.1
6.788	6.788 [e]		0	48300	94.7 ± 22.1	45	43.6
7.017	7.021 [e]	2	1	71	59.6 ± 10.9	36	38.1
7.048	7.053 [e]		0	3477	64.0 ± 16.6	35	33.9
7.173	7.178	1	1	63	33.5 ± 5.5	15	24.9
7.400	7.398	1	1	140	63.8 ± 3.3	30	31.7
7.473	7.510 [e]		0	5195	50.1 ± 5.4	36	34.8
7.812	7.815	1	1	94	53.0 ± 2.8	24	28.6
7.960	7.944	1	1	57	28.7 ± 3.4	12	23.9
8.186	8.190 [e]		0	14370	98.3 ± 10.0	55	53.2
8.226	8.223 [e]	1	1	81	12.8 ± 6.1	21	27.2
8.401	8.403	1	1	100	44.9 ± 3.1	25	29.1
8.846	8.847 [e]		0	3138	53.3 ± 14.3	39	37.7
8.857	8.865 [e]	1	1	85	49.8 [f]	22	27.7
9.115	9.118	1	1	120	64.3 ± 9.0	28	30.6
9.239	9.236 [e]	1	1	89	22.4 [f]	23	28.1
9.296		1	1	52		9	22.9
9.342	9.330 [e]	1	1	106	47.6 ± 15.1	26	29.6
9.372	9.368 [e]		0	36290	45.6 ± 15.0	36	34.8
9.530	9.544	1	1	61	91.2 ± 9.5	14	24.6
9.557		2	1	66		32	36.5
9.735	9.740		0	47930	105.4 ± 17.1	77	74.5
9.956	9.945 [e]	1	1	133	82.9 ± 7.6	19	26.4
10.04	10.02 [e]	1	1	64	48.5 ± 8.0	21	27.2
10.12	10.11 [e]	2	1	150	126.5 ± 8.0	61	52.5
10.71	10.69 [e]	2	1	66	55.8 [f]	73	36.7
10.71	10.69 [e]		0	58500	115.3 ± 12.2	46	44.5
11.24	11.25 [e]		0	18590	117.2 ± 10.0	64	61.9
11.39	11.40 [e]	2	1	120	79.7 ± 7.1	60	51.7
11.64	11.64 [e]		0	15930	68.1 ± 11.5	31	29.9
11.72	11.73 [e]	1	1	53	39.1 ± 7.9	33	23.6
	12.07 [e]	1	1	100 [d]	48.5 ± 6.8		
12.18	12.19 [e]		0	4322	64.5 ± 9.8		
	12.45	1	1	120 [d]	42.7 ± 7.9		
	12.65	1	1	120 [d]	40.1 ± 7.4		
	13.14 [e]	1	1	130 [d]	27.6 [f]		
13.24	13.23 [e]		0	61820	89.9 ± 14.7		
	13.38 [e]	1	1	140 [d]	109.3 ± 10.1		

TABLE II. *(Continued).*

Resonance energy (keV)		g	l	$g\Gamma_n$ [a]	Resonance area [b] (meV)		
Ref. [10]	This work			(meV)	This work	Ref. [5]	Ref. [10] [c]
13.58	13.56 [e]		0	14180	123.8 ± 13.2		
	13.83 [e]	1	1	150 [d]	42.5 ± 8.4		
14.00	13.98 [e]		0	41000	92.1 ± 15.1		
14.48	14.47		0	2917	104.5 ± 11.8		
	14.82 [e]	1	1	150 [d]	42.9 [f]		
	15.00	1	1	184 [d]	106.1 ± 9.4		
15.24	15.25		0	2270	94.7 ± 9.3		
	15.50	2	1	185 [d]	126.7 ± 9.2		
	15.82	1	1	200 [d]	113.5 ± 11.0		
	16.18 [e]	1	1	180 [d]	78.0 ± 13.2		
16.32	16.30 [e]		0	58710	194.5 ± 22.8		
16.72	16.70 [e]		0	26200	93.8 ± 19.4		
16.83	16.82 [e]		0	33900	108.1 ± 20.5		
	17.33 [e]	1	1	200 [d]	84.2 ± 12.7		
17.54	17.52 [e]		0	10840	117.2 ± 15.0		
	17.57 [e]	1	1	200 [d]	82.3 [f]		
	17.98 [e]	1	1	210 [d]	102.5 ± 12.2		
18.19	18.18 [e]		0	8432	146.1 ± 23.0		
	18.30 [e]	1	1	220 [d]	73.5 ± 16.6		
18.43	18.50 [e]		0	40830	177.6 ± 17.7		
	18.95	1	1	240 [d]	98.0 ± 11.5		
	19.20	1	1	240 [d]	102.7 ± 11.5		
19.41	19.48 [e]		0	28590	104.6 ± 18.2		
	19.63 [e]	1	1	260 [d]	88.5 ± 13.8		
	19.90	1	1	260 [d]	104.3 ± 11.1		

[a]Values for g, l, and $g\Gamma_n$ adopted from the JENDL-3 evaluation.
[b]$A_\gamma = g\Gamma_n\Gamma_\gamma/(\Gamma_n+\Gamma_\gamma)$.
[c]Capture area of p-wave resonances calculated with an average capture width of 41 meV.
[d]Calculated according to Eq. (2); g and l arbitrarily set to unity.
[e]Resonance energy was taken as fixed parameter.
[f]Adopted as fixed parameter from Ref. [12].

$$g_J\langle\Gamma_n\rangle_{lJ} = \nu_{lJ} g_J D_J S_l \sqrt{E} v_l(E), \tag{1}$$

where the quantities g, D, S, ν, and v_l denote the statistical weight factor, the mean level spacing, the strength function, the number of possible channel spins, and the penetrability factor for the respective orbital angular momenta l. For p-wave resonances, this expression reduces to

$$g\langle\Gamma_n\rangle_1 = D_s S_1 \sqrt{E} \frac{(kR)^2}{1+(kR)^2}. \tag{2}$$

The reliability of the resonance areas A_γ depends on the available experimental information on neutron widths and spins. For the two neodymium isotopes under consideration the situation is much more favorable compared to the previously investigated tin and barium isotopes [3,4]. As discussed in these references, the systematic uncertainties of the resonance analysis depend on the quality of the available s-wave neutron widths. These data are most critical for ^{144}Nd due to its large s-wave strength. For both investigated isotopes the neutron widths of all s-wave resonances are provided by the JENDL-3 evaluation [10]. For p-wave resonances all g and $g\Gamma_n$ values are known for ^{142}Nd while for ^{144}Nd this information exists up to 11.7 keV. At higher energies, the $g\Gamma_n$ were calculated according to Eq. (2) and the g values were arbitrarily set to unity. The systematic uncertainties due to lacking neutron widths and g values can be neglected in the present study.

In a first step the energies of well isolated resonances were determined. The comparison with a recent high resolution experiment by Guber [12] showed that the energy differences are linearly increasing with resonance energy. Hence, this relation was used to calculate the resonance energies for all unresolved multiplets consistent with the energy scale of Ref. [12]. These energies were then adopted as fixed parameters in the fits. In the second step, all resonance areas were determined. These results are given in Tables I and II; the preliminary data of Guber can be found in Ref. [13]. For a few exceptions (2 cases in ^{142}Nd and 6 in ^{144}Nd, mostly for p-wave resonances close to an s-wave resonance), the p-wave areas of Ref. [12] were directly used as fixed input parameters to obtain a more reliable fit of the nearby s-wave resonance. The quoted statistical uncertainties are those provided by the FANAC code. The experimental capture yield of ^{144}Nd and the FANAC fit are compared in Fig. 1, the respective figure for ^{142}Nd can be found in Ref. [13].

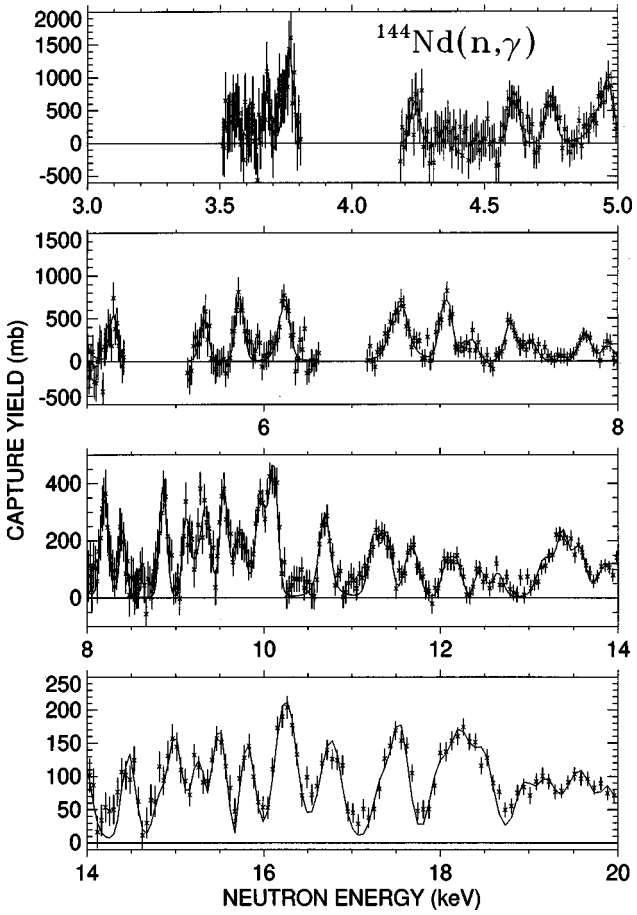

FIG. 1. The neutron capture yield of ^{144}Nd and the corresponding FANAC fit.

The gaps in the data correspond to energy intervals without significant resonances.

If the resonance energies are compared with the values given by Mughabghab *et al.* [5], JENDL-3 [10], and Guber [12], one finds that around 4 keV all data sets agree on average to better than 6 eV for ^{142}Nd and to better than 10 eV for ^{144}Nd. With increasing energy, there are linearly increasing differences. At an energy of 15 keV, these differences have reached values (in the order of the above citations) of 30, 100, 50 eV for ^{142}Nd and of 0, 0, 60 eV for ^{144}Nd, respectively. These deviations are compatible with an uncertainty of $\sim$1 mm in the flight path of the present experiment which translates into a 40 eV uncertainty in the resonance energy at 15 keV. The large discrepancy with respect to the JENDL-3 data for ^{142}Nd is somewhat surprising since the data sets of Refs. [5,10] are based on the same experimental results [14].

As far as the resonance areas are concerned there is good agreement for the p-wave resonances of ^{142}Nd. The sum of all p-wave areas obtained in the various experiments agrees within 4%, and the scatter of individual resonance areas is in most cases less than $\pm 20\%$, compatible with the statistical uncertainties and with the fact that the limited energy resolution of the present experiment hampers the separation of multiplets.

For the s-wave resonances in ^{142}Nd the situation is different, however. Though the sum of all s-wave areas exceeds the value of the other data sets by only $\sim$7%, the individual

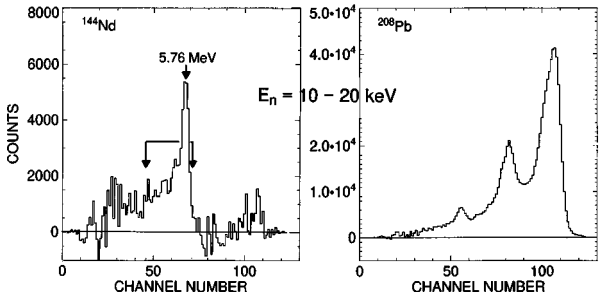

FIG. 2. Sum energy spectra of capture events in the ^{144}Nd sample and in the ^{208}Pb scattering sample illustrating the proper correction of background from scattered neutrons and from isotopic impurities. The data refer to 1 run of the experiment and the neutron energy range from 10 to 20 keV. The region marked by arrows was used for evaluating the ^{144}Nd cross section.

areas scatter by more than a factor of two. There seem to be several systematic effects involved which cancel out in the sum. The most prominent examples are the resonances at 3.382, 9.019, 13.66, and 16.26 keV. The resonance areas of the first 2 resonances, which exhibit very small neutron widths, are systematically larger by 50 to 100% compared to the values of Refs. [5,10,12], whereas the areas of the two other resonances, which have very large neutron widths, are lower by nearly a factor of two. These discrepancies for s-wave resonances might arise in experiments using long flight paths and the pulse height weighting technique due to problems with the neutron sensitivity and/or with the weighting function in case of resonances with very hard capture γ-ray spectra. Though these problems have been widely discussed in the past they seem to persist, in particular in case of neutron magic nuclei such as ^{142}Nd, which are likely showing hard capture γ-ray spectra.

The comparably strong resonance at 7.627 keV is not listed in the older data, but has also been found by Guber [12]. Adopting their s-wave assignment and assuming a neutron width of 600 meV according to the similar shape compared to neighboring resonances yields a resonance area of 82.1 ± 4.9 meV. However, even an extreme neutron width of 8000 meV, estimated via Eq. (1), has little impact on the resonance area, which then reduces to 76.2 meV.

In the case of ^{144}Nd the situation is more complex. The sum of all present p-wave and s-wave areas are 60% and 70% higher than the respective values in the compilations of Mughabghab [5] and JENDL-3 [10] which are both based on the experiment by Musgrove *et al.* [14], indicating a severe normalization uncertainty. Compared to the work of Guber [12] our results are systematically higher by 10% for the p-wave, but 33% for the s-wave resonances in the range below 15 keV. Here again differences up to a factor of two occur for individual resonances but—in contrast to ^{142}Nd—both types of s-wave resonances, with very low (e.g., at 2.762, 3.749, 4.738, 14.48 keV) and very high (6.788, 9.735, 10.712 keV) neutron widths are higher in the present experiment. There is no clear correlation with the neutron width, however, since other resonances in both categories agree reasonably well.

Due to the very large s-wave strength function of ^{144}Nd, the cross section is dominated by resonances with $\Gamma_n \geqslant 10$ eV. Therefore, the prompt neutron sensitivity of the experi-

TABLE III. Averaged capture cross sections of ^{142}Nd and ^{144}Nd.

Neutron energy	Capture cross section (mb) [a]					
	^{142}Nd			^{144}Nd		
(keV)	This work	Ref. [2]	Ref. [12]	This work	Ref. [2]	Ref. [12]
3–5	109.4 ± 5.5	74.7 ± 25 [b]	90.8	205.5 ± 12	255.9 ± 35	186.6
5–7.5	118.7 ± 3.5	93.0 ± 9.0	121.6	176.0 ± 10	207.8 ± 14	149.5
7.5–10	96.6 ± 2.3	80.4 ± 5.3	77.5	158.9 ± 6.6	179.3 ± 8.1	120.8
10–12.5	44.8 ± 1.4	41.8 ± 3.4	44.2	120.6 ± 4.2	110.6 ± 4.8	90.8
12.5–15	68.2 ± 3.3	62.2 ± 2.6	70.9	93.3 ± 4.0	86.7 ± 3.5	78.4
15–20	34.6 ± 1.0	35.0 ± 1.3		99.2 ± 3.1	96.9 ± 1.7	

[a]Including statistical uncertainties.

[b]This energy bin was not used in the evaluation of Maxwellian averaged cross sections in Ref. [2].

mental setup has to be carefully considered. In the present analysis, this problem is controlled in three ways: (i) Due to the short primary neutron flight path of 78 cm and the additional 10 cm distance between the sample and the individual modules of the 4π BaF_2 detector, background from scattered neutrons is spread out over a large TOF interval that is delayed compared to the prompt γ-signal from the respective resonance. (ii) The probability for capturing a neutron immediately after scattering is properly considered by the FANAC code. (iii) Any differences in the capture γ-ray spectra of individual resonances, that are difficult to consider in experiments using the pulse height weighting technique, are automatically accounted for in the 4π detector.

This is illustrated by the γ-spectrum of capture events in ^{144}Nd (Fig. 2) that was determined for the neutron energy range from 10–20 keV, where the cross section is dominated by broad s-wave resonances. The data of one of the experimental runs are plotted together with the respective spectrum of the ^{208}Pb scattering sample, demonstrating the reliability of the background correction for scattered neutrons. In addition to the scattering correction, which eliminates the pronounced peak around channel 107 due to captures in the odd Ba isotopes of the scintillator, the correction for isotopic impurities accounts for capture events in ^{143}Nd and ^{145}Nd, which are otherwise expected as a common line at channel $\sim$90.

III. RESULTS

The average capture cross sections calculated from the resonance parameters listed in Tables I and II agree within the quoted statistical uncertainties with the previous analysis [2] (see Table III). This confirms the proper treatment of the background due to scattered neutrons, which is comparably large at low energies. For two entries in Table III (^{142}Nd, 5–7.5 keV and 7.5–10 keV) the difference with the previous analysis reaches the 2σ level, but this occurs in regions with few resonances, where the large gaps between resonances were adding additional background to the first analysis.

For ^{142}Nd, excellent agreement is found with the data of Guber [12]. The 25% difference in the interval from 7.5–10 keV is almost completely due to the s-wave resonance at 9.019 keV which has a 2.2 times larger area according to the present experiment. In case of ^{144}Nd, however, there are systematic differences of up to 30% in the energy interval from 7.5–12.5 keV, a region where broad s-wave resonances are clearly dominating the cross section.

Based on the results of Table III revised Maxwellian averaged cross sections for thermal energies between 10 and 30 keV are given in Table IV together with the previous results and the data of Ref. [15]. The differences between the first analysis and the present results are accounted for by the quoted uncertainties, which are now slightly smaller. The comparison with the cross sections of Guber *et al.* [15] shows the same picture as for the average cross sections: perfect agreement for ^{142}Nd, but a significant discrepancy for ^{144}Nd at low thermal energies, due to the problem with the s-wave resonances below 12.5 keV.

IV. CONCLUSIONS

The improved analysis of the neutron capture cross sections of ^{142}Nd and ^{144}Nd in the energy range from 2.8–20 keV yielded the resonance areas of 52 and 78 resonances,

TABLE IV. Maxwellian averaged neutron capture cross sections of ^{142}Nd and ^{144}Nd.

Thermal energy	$\langle\sigma v\rangle/v_T$ (mb) [a]					
	^{142}Nd			^{144}Nd		
(keV)	This work	Ref. [2]	Ref. [15]	This work	Ref. [2]	Ref. [15]
10	65.1 ± 1.9	60.1 ± 1.9	65.8 ± 2.9	147.0 ± 4.5	153.1 ± 4.5	122.2 ± 5.4
12	58.4 ± 1.6	54.4 ± 1.6		131.3 ± 3.6	135.8 ± 3.6	
20	43.4 ± 0.9	41.5 ± 0.9	44.2 ± 3.0	98.9 ± 2.1	100.7 ± 2.1	86.7 ± 6.1
25	38.4 ± 0.8	37.1 ± 0.8		88.5 ± 1.7	89.6 ± 1.7	
30	35.0 ± 0.7	34.0 ± 0.7	36.6 ± 3.0	81.3 ± 1.5	82.1 ± 1.5	73.2 ± 6.1

[a]Total uncertainty, but without the 1.5% systematic uncertainty of the gold reference cross section.

respectively. The resulting averaged cross sections are in good agreement with the first analysis which was based on the observed capture yields only [2]. This agreement confirms the reliable background subtraction in experiments with the Karlsruhe 4π BaF_2 detector. The Maxwellian averaged cross sections could be slightly improved for low kT values but remain essentially unchanged. Therefore, the s-process studies based on the cross sections of Refs. [2,16] are not affected.

ACKNOWLEDGMENT

The help of F.H. Fröhner in using the FANAC code is gratefully appreciated.

[1] Z. Y. Bao and F. Käppeler, At. Data Nucl. Data Tables **36**, 411 (1987).
[2] K. Wisshak, F. Voss, F. Käppeler, L. Kazakov, and G. Reffo, Report No. FZKA–5967, Forschungszentrum Karlsruhe, 1997; Phys. Rev. C **57**, 391 (1998).
[3] F. Voss, K. Wisshak, and F. Käppeler, Phys. Rev. C **52**, 1102 (1995).
[4] K. Wisshak, F. Voss, and F. Käppeler, Phys. Rev. C **54**, 2732 (1996).
[5] J. F. Mughabghab, M. Divadeenam, and N. E. Holden, *Neutron Cross Sections* (Academic Press, New York, 1984), Vol. 1, Pt. A.
[6] F. Käppeler, R. Gallino, M. Busso, G. Picchio, and C. Raiteri, Astrophys. J. **354**, 630 (1990).
[7] O. Straniero, R. Gallino, M. Busso, A. Chieffi, C. M. Raiteri, M. Limongi, and M. Salaris, Astrophys. J. **440**, L85 (1995).
[8] K. Wisshak, K. Guber, F. Käppeler, J. Krisch, H. Müller, G. Rupp, and F. Voss, Nucl. Instrum. Methods Phys. Res. A **292**, 595 (1990).
[9] F. H. Fröhner, Report No. KfK-2145, Kernforschungszentrum Karlsruhe, 1977.
[10] Japanese evaluated nuclear data library JENDL-3 as obtained via internet from Brookhaven Nuclear Data Center 1997.
[11] F.H. Fröhner, Report No. GA-8380, Gulf General Atomic, 1968.
[12] K. H. Guber (private communication).
[13] K. Wisshak, F. Voss, and F. Käppeler, Report No. FZKA-5968, Forschungszentrum Karlsruhe, 1997.
[14] A. R. de L. Musgrove, B. J. Allen, J. W. Boldeman, and R. L. Macklin, *Proceedings of the International Conference on Neutron Physics and Nuclear Data for Reactors and Other Applied Purposes*, Harwell, UK, 1978 (OECD Nuclear Energy Agency, Paris, France, 1978), p. 449 and report AAEC/E401, Australian Atomic Energy Commission (1976).
[15] K. H. Guber, R. R. Spencer, P. E. Koehler, and R. R. Winters, Phys. Rev. Lett. **78**, 2704 (1997).
[16] K. Wisshak, F. Voss, F. Käppeler, and L. Kazakov, Proceedings of the International Conference on Nuclei in the Cosmos 96, Notre Dame (1996) [Nucl. Phys. **A621**, 270c (1997)].